

Kernel Estimation from Salient Structure for Robust Motion Deblurring[☆]

Jinshan Pan^a, Risheng Liu^a, Zhixun Su^{a,*}, Xianfeng Gu^b

^a*School of Mathematical Sciences, Dalian University of Technology, Dalian, China
116024*

^b*Department of Computer Science, Stony Brook University, Stony Brook, USA*

Abstract

Blind image deblurring algorithms have been improving steadily in the past years. Most state-of-the-art algorithms, however, still cannot perform perfectly in challenging cases, especially in large blur setting. In this paper, we focus on how to estimate a good kernel estimate from a single blurred image based on the image structure. We found that image details caused by blurring could adversely affect the kernel estimation, especially when the blur kernel is large. One effective way to eliminate these details is to apply image denoising model based on the Total Variation (TV). First, we developed a novel method for computing image structures based on TV model, such that the structures undermining the kernel estimation will be removed. Second, to mitigate the possible adverse effect of salient edges and improve the robustness of kernel estimation, we applied a gradient selection method. Third, we proposed a novel kernel estimation method, which is capable of

[☆]This work is partially supported by the National Natural Science Foundation of China under Contract No.s U0935004 and 61173103.

*Corresponding author. Tel.: +86-411 84708351-8020.

Email addresses: sdluran@gmail.com (Jinshan Pan), rsliu0705@gmail.com (Risheng Liu), zxsu@dlut.edu.cn (Zhixun Su), gu@cs.sunysb.edu (Xianfeng Gu)

preserving the continuity and sparsity of the kernel and reducing the noises. Finally, we developed an adaptive weighted spatial prior, for the purpose of preserving sharp edges in latent image restoration. The effectiveness of our method is demonstrated by experiments on various kinds of challenging examples.

Keywords: Motion deblurring, kernel estimation, image restoration, salient structures/edges

1. Introduction

Motion blur is a common problem caused by camera shake during the exposure period. It gains considerable attention in recent years due to its involvement of many challenges in problem formulation, regularization, and optimization. It is usually modeled as a linear image degradation process:

$$B = I * k + \varepsilon, \quad (1)$$

where B , I , k and ε represent the blurred image, latent image, blur kernel (a.k.a. point spread function (PSF)) and the additive noise, respectively. $*$ denotes the convolution operator. It is a well-known ill-posed inverse problem, which requires regularization to alleviate its ill-posedness and stabilize the solution.

Significant progress has been made [1, 2, 3, 4, 5, 6, 7]. The success of these methods comes from the sharp edge restoration and noise suppression in smooth regions, which enable accurate kernel estimation.

However, blurred image with some complex structures or large blur will fail most of the current state-of-the-art blind deblurring methods. Taking

Fig. 1(a) as an example, due to the camera shake, the motion blur is very large, in addition, the blurred image also contains complex structures. As shown in Fig. 1(b) ~ (f), some state-of-the-art methods [1, 2, 3, 6, 7] cannot restore or select useful sharp edges for kernel estimation due to the large blur and complex structures, thus, the correct blur kernels are not obtained. This inevitably makes the final deblurred results unreliable.

We address this issue and propose a new kernel estimation method based on the reliable structures. Our method is a new selection scheme to select reliable structures adapting to the image characteristics. Thus, it is able to get useful sharp edges for kernel estimation. Our deblurred result shown in Fig. 1(g) contains fine textures, and the kernel estimate is also better than others.

Based on above analysis, we develop several strategies which are significantly different from previous works in the following aspects.

1. We observe that the image structural information plays a critical role in the deblurring process. Therefore, we develop a novel structure selection method which can choose reliable structures effectively adapting to the image characteristics.
2. Conventional kernel estimation methods use hard thresholding to the kernel elements to remove noise, which damage the kernel structures (e.g., Continuity). Our method overcomes the disadvantages of existing ones to preserve the sparsity and continuity, remove noise in kernels.
3. We introduce a simple adaptive regularization term that combines our final structures to guide the latent image restoration, which preserves sharp edges effectively.

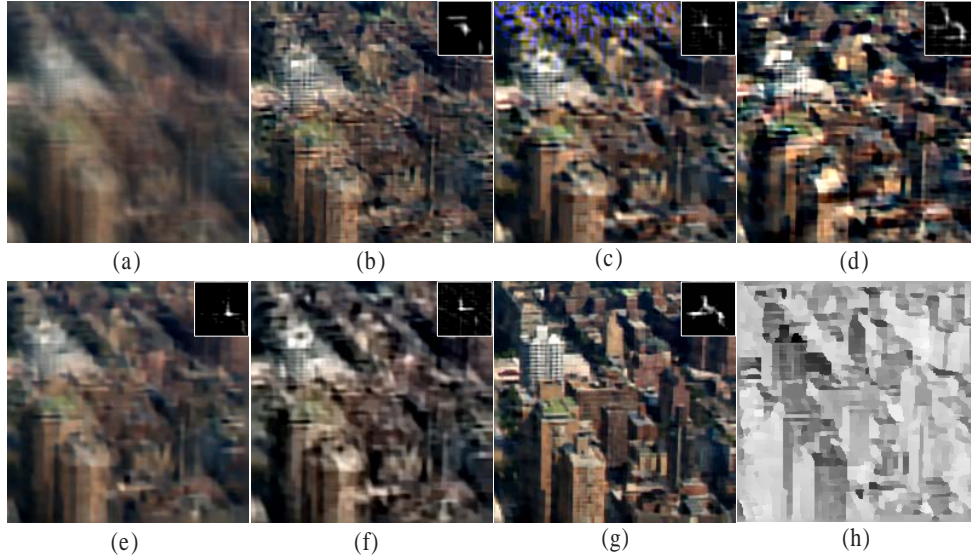


Figure 1: A challenging example that most current state-of-the-art methods fail. (a) Blurred image. (b) Result of Shan *et al.* [2]. (c) Result of Cho and Lee [1]. (d) Result of Xu and Jia [3]. (e) Result of Levin *et al.* [7]. (f) Result of Krishnan *et al.* [6]. (g) Our result. (h) Our final salient edges ∇S visualized by using Poisson reconstruction method. The size of motion blur kernel is 45×45 .

We applied our method to some challenging examples, such as the blurred images with some complex structures, or with large blur kernels. We found that it is able to provide reliable kernel estimates.

2. Related Work

Previous image deblurring methods can be roughly separated into two categories: non-blind deconvolution and blind deconvolution. In this paper, we mainly focus on blind deconvolution.

In blind deconvolution, early approaches usually impose constraints on motion blur kernel and used parameterized forms for the kernels [8, 9]. Re-

cently, Fergus *et al.* [4] adopted a zero-mean Mixture of Gaussian to fit for natural image gradients, and a variational Bayesian method was employed to deblur an image. Shan *et al.* [2] used a certain parametric model to approximate the heavy-tailed natural image prior. Levin *et al.* [10] illustrated the limitation of the simple maximum a-posteriori (MAP) approach, and efficient marginal likelihood approximation was introduced in [7]. However, the kernel estimates of these methods contain some noises. The hard thresholding to the kernel elements method will destroy the inherent structure of kernels.

Another group methods [1, 3, 5] employed an explicit edge prediction step for kernel estimation. Cho and Lee [1] used bilateral filtering together with shock filtering to predict sharp edges iteratively, and then selected the salient edges for kernel estimation. However, the Gaussian priors used in this method can not keep the sparsity of the motion blur kernel and the image structure. The final result usually contains noise. Xu and Jia [3] proposed an effective mask computation algorithm to adaptively select useful edges for kernel estimation, the kernel refinement was achieved by using iterative support detection (ISD) method [11]. However, this method only considered the sparsity of the motion blur kernel, and the estimated kernel also contains some noises occasionally.

In the final deblurring stage, which is also known as the non-blind image deconvolution. The well-known method is the Richardson-Lucy deconvolution [12]. Recent works mainly focus on the natural image statistics [2, 13] to keep the properties of latent images and suppress ringing artifacts. The works in [3, 14] used TV regularization to restore latent images, while the isotropic TV regularization will result in stair-casing effect. Krishnan *et al.* [6] used

normalized sparsity measure to restore latent images; this regularizer leads to the non-convex problem and needs to special method to solve it. In this paper, we make use of our final structure to guide latent images restoration which preserves more details of latent images.

3. Motion Deblurring from Salient Structure

We find that different extraction of structure leads to different deblurred results, and extracting reliable structure is critical to deblurring. Thus, we focus on extracting more reliable structures, which is achieved by several key steps. First, we extract the main image structure (the first part of the red box in Fig. 2); then a shock filter is applied to get the enhanced structure (the second part of the red box in Fig. 2). Finally, some salient edges with large pixel values will be selected for the kernel estimation (the third part of the red box in Fig. 2). The details of this process for extracting salient edges will be discussed in Section 3.1. The flowchart shown in Fig. 2 illustrates our deblurring process in details.

3.1. Constructing Salient Structure

Our method for adaptively selecting salient edges mainly relies on the idea of structure-texture decomposition method [15]. For an image I with pixel intensity value $I(x)$, the structure part is given by the optimizer of the following energy

$$\min_{I_s} \|\nabla I_s\|_2 + \frac{1}{2\theta} \|I_s - I\|_2^2. \quad (2)$$

where θ is adjustable parameter. The image $I(x)$ is decomposed into the structure component I_s (shown in Fig. 3(c)) and the texture component

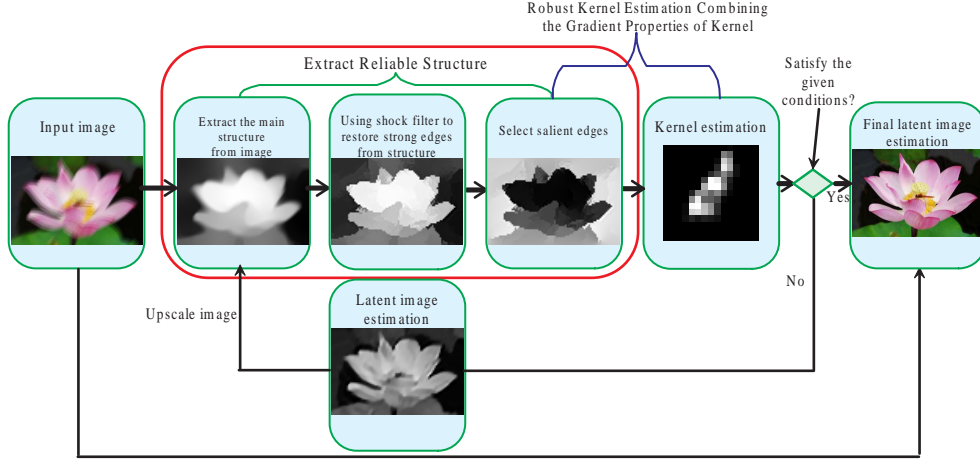


Figure 2: The process of our algorithm.

$I_T = I - I_s$ (shown in Fig. 3(b)). The component I_s contains the major large objects in the image while I_T includes fine-scale details and some noises.

Fig. 3(f) demonstrates that the accuracy of kernel estimate is greatly improved by performing model (2). However, model (2) may lead to stair-casing effect in smooth area. This will cause gradient distortion and introduce inaccuracy for blur kernel estimation. A simple way to mitigate this effect is to adjust the value of θ to be large in smooth area, and small near the edges. Therefore, we employ an adaptive function defined in Eq. (3) to achieve this goal.

$$r(\mathbf{x}) = \frac{\|\sum_{\mathbf{y} \in N_h(\mathbf{x})} \nabla B(\mathbf{y})\|_2}{\sum_{\mathbf{y} \in N_h(\mathbf{x})} \|\nabla B(\mathbf{y})\|_2 + 0.5}, \quad (3)$$

where B is the blurred image, and $N_h(\mathbf{x})$ is a $h \times h$ window centered at pixel \mathbf{x} . A small value r implies that the local region is flat, whereas large value r implies existing strong image structures in the local window. This equation is first employed by [3] to remove some narrow strips that may undermine

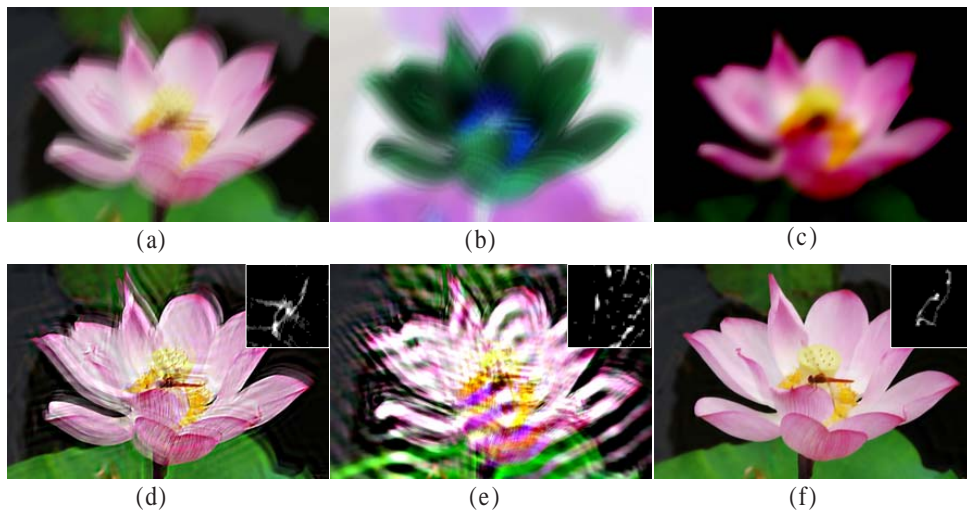


Figure 3: Different structures leading to different deblurred results. (a) Blurred image. (b) Texture component I_T . (c) Structure component I_s . (d) Results without performing model (2). (e) Results by using I_T in the process of kernel estimation. (f) Results by using I_s in the process of kernel estimation.

the kernel estimation.

With this adaptive function r , we reformulate model (2) as follows,

$$\min_{I_s} \|\nabla I_s\|_2 + \frac{1}{2\theta\omega(\mathbf{x})} \|I_s - I\|_2^2, \quad (4)$$

where $\omega(\mathbf{x}) = \exp(-\|r(\mathbf{x})\|^{0.8})$.

According to above analysis, model (4) keeps the similar advantages to the method [3]. It also has strong penalty to these areas which are flat or contain narrow strips as well. Model (4), however, can adaptively obtain the intrinsic image structures.

As shown in Fig. 4(a), the blurred image contains some complex structures, which may have detrimental effects on kernel estimation. The kernel estimation result shown in Fig. 4(c) illustrates the effectiveness of our im-



Figure 4: Comparison of results using model (2) and our improved model (4). (a) Blurred image and truth kernel. (b) Result with model (2). (c) Result with model (4). (d) Result of [3]. The results (including the kernel estimate and deblurred result) of our improved model (4) in (c) performs better than others.

proved model (4), while the deblurred result of [3] still contains some blur due to the imperfect kernel estimation result¹.

After computing the structure I_s , we apply the shock filter to enhance the structure of I_s and select reliable salient edges to guide the kernel estimation. Shock filter is an effective tool to restore strong edges from the blurred images, and it can be achieved by solving the following PDE problem [16].

$$I_t = -\text{sign}(\Delta I) \|\nabla I\|_2, \quad (5)$$

where ∇I is the gradient of image, $\Delta I = I_x^2 I_{xx} + 2I_x I_y I_{xy} + I_y^2 I_{yy}$.

Finally, we use unit binary mask function $H(\mathbf{x}, y)$ to refine the structure and mitigate the possible adverse effect to the kernel estimation.

$$H(\mathbf{x}, t) = \begin{cases} 1 & x_i \geq t \\ 0 & \text{otherwise} \end{cases}. \quad (6)$$

To increase the robustness of kernel estimation, the final salient edges ∇S can be obtained from

$$\nabla S = \nabla I_{ss} H(\mathbf{G}, t), \quad (7)$$

¹More comparable results can be found in our supplementary material.

where $\mathbf{G} = (\|\nabla I_{ss}\|_2, \|I_{ss}^x\|_1/5\sqrt{2}, \|I_{ss}^y\|_1/5\sqrt{2})$, I_{ss} denotes the shock filtered structure I_s , I_{ss}^x , I_{ss}^y denote horizontal and vertical derivatives, respectively, and t is a threshold of $\|\nabla I_{ss}\|_2$ which is determined by the size of blur kernel. By applying Eq. (7), some noise existing in the ∇I_{ss} will be eliminated. Thus, only the salient edges with large values have influences on the kernel estimation. The effectiveness of salient edges will be detailed in Section 3.3.

3.2. Robust Kernel Estimation from Salient Structure

After sharp edges selection, we can estimate the motion blur kernel with ∇S . The traditional model for motion blur kernel estimation is as follows,

$$\begin{aligned} \min_k \quad & \|\nabla B - k * \nabla S\|_2^2 + \gamma \|k\|_\alpha^\alpha, \\ \text{s.t.} \quad & k(x, y) \geq 0; \quad \sum_{\{x,y\}} k(x, y) = 1. \end{aligned} \quad (8)$$

Although model (8) can preserve the sparsity prior effectively, it does not ensure the continuity of blur kernel, and sometimes induces noisy kernel estimates, as shown in Fig. 5(e). Noise in the kernel estimate will lead to the inaccurate deblurred result (shown in Fig. 5(b)).

One important observation of the kernel is that its gradient is extremely sparse, so the traditional gradient constraints of kernels will not keep the property of kernel well, and these constraints sometimes damage the shape of kernel. The kernel estimate shown in Fig. 5(d), which is generated by

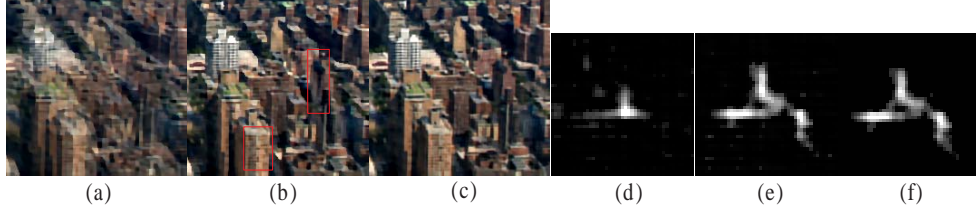


Figure 5: Comparison of results using different spatial priors of motion blur kernel. (a) and (d) are results by using model (9). (b) and (e) are results by using model (8). (c) and (f) are our estimated results. Deblurred result in (c) outperform result in (b) (e.g., the parts in the red boxes).

using model²

$$\begin{aligned} \min_k \quad & \|\nabla B - k * \nabla S\|_2^2 + \gamma \|k\|_\alpha^\alpha + \|\nabla k\|_\nu^\nu, \\ \text{s.t.} \quad & k(x, y) \geq 0; \quad \sum_{\{x, y\}} k(x, y) = 1. \end{aligned} \quad (9)$$

with the parameter $\alpha = \nu = 0.5$, demonstrates this case. We can see that it fails to produce correct results.

Based on above analysis, we introduce an effective gradient constraint to preserve the continuity and remove noise in the blur kernels. The measure is expressed as,

$$\mathcal{C}(k) = \#\{(x, y) \mid |\partial_x k(x, y)| + |\partial_y k(x, y)| \neq 0\}. \quad (10)$$

$\mathcal{C}(k)$ counts the number of position (x, y) which satisfies $|\partial_x k(x, y)| + |\partial_y k(x, y)| \neq 0$. It can make the kernel sparse and preserve the continuity of the kernel. With this constraint, our final energy for kernel estimation is

²This kernel estimation model is also employed in [17].

formulated as,

$$\begin{aligned} \min_k & \|\nabla B - k * \nabla S\|_2^2 + \gamma \|k\|_\alpha^\alpha + \mu \mathcal{C}(k), \\ \text{s.t.} \quad & k(x, y) \geq 0; \quad \sum_{\{x, y\}} k(x, y) = 1. \end{aligned} \quad (11)$$

where the parameter μ controls the smoothness of k .

Note that model (11) is hard to be minimized directly due to involving a discrete counting metric. Similar to the strategy of [18], we approximate it by alternately minimizing

$$\begin{aligned} \min_k & \|\nabla B - k * \nabla S\|_2^2 + \gamma \|k\|_\alpha^\alpha, \\ \text{s.t.} \quad & k(x, y) \geq 0; \quad \sum_{\{x, y\}} k(x, y) = 1, \end{aligned} \quad (12)$$

and

$$\min_{\hat{k}} \|\hat{k} - k\|_2^2 + \mu \mathcal{C}(\hat{k}). \quad (13)$$

Note that model (12) can be optimized by using iterative reweighted least square (IRLS) method [13], while model (13) is L_0 gradient minimization problem which is proposed by [19]. In this work, we employ the alternating optimization method of [19] to solve model (13). Alg. 1 illustrates the implementation details of model (11).

We set $Itr = 5$, and $\alpha = 0.5$ in our experiment. The parameter μ is chosen according to the size of kernels. Fig. 5(d) \sim (f) show the kernel estimation results with different spatial priors, respectively. Our deblurred result and kernel estimate shown in Fig. 5(c) and (f), respectively, outperform others.

Interim Latent Image Estimation: In this deconvolution stage, we focus on the sharp edges restoration from the blurred image, thus, we employ

Algorithm 1 Robust Kernel Estimation

Input: Blurred image B , salient edges ∇S , and the initial values of k from previous iterations;

for $i = 1 \rightarrow Itr$ (Itr : number of iterations) **do**

 Solve for k by minimizing model (12);

 Solve for \hat{k} by minimizing model (13);

$k \leftarrow \hat{k}$;

end for

Output: Blur kernel k .

the anisotropic TV model to guide the latent image restoration. It can be written as,

$$\min_I \|B - k * I\|_2^2 + \lambda_c \|\nabla I\|_1. \quad (14)$$

3.3. More Analysis on Kernel Estimation

Inaccurate sharp edges will induce noisy or even wrong kernel estimates, which furthermore deteriorate the final recovered images. In this subsection, we demonstrate the effectiveness of our salient edges ∇S and provide some analysis about kernel estimation method via some examples.

As pointed out in Introduction, image details will damage the kernel estimation, thus, we proposed to estimate blur kernels by using salient edges ∇S . The salient edges ∇S are extracted from interim latent images, and it contains the gradient with large pixel values. To verify the validity of ∇S , we perform several experiments by using the data from [10]. Furthermore, to emphasize the fact that tiny structures may damage the kernel estimation, we select the data with rich details such as trees and grass from [10] (shown

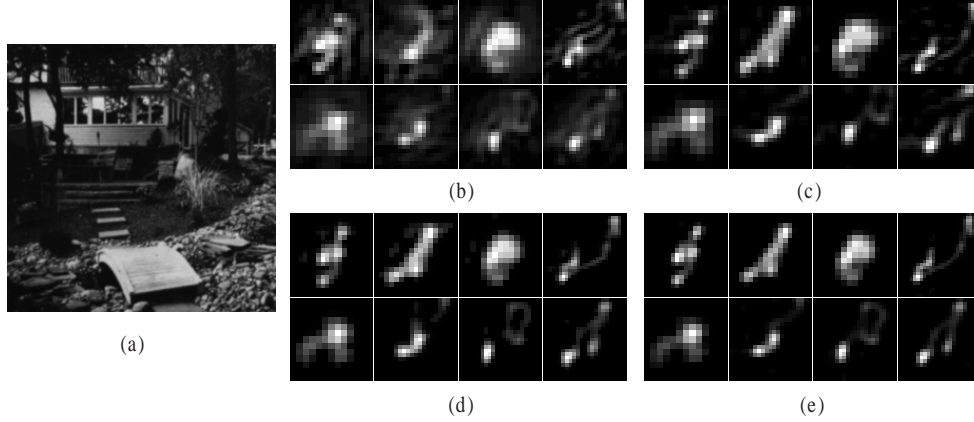


Figure 6: Comparison of results with and without model (4). (a) The ground truth image. (b) Kernel estimates without adopting model (4). (c) Kernel estimates of [1]. (d) Kernel estimates of [3]. (e) Kernel estimates with model (4).

in Fig. 6(a)).

Fig. 6 shows an example where we apply model (4) in the kernel estimation process. Due to the proposed structure selection mechanism, the kernel estimates (shown in Fig. 6 (e)) outperform the results without adopting this strategy (i.e., Fig. 6 (b)). Compared with other structure selection methods [1, 3], our method as a whole outperforms better. This is mainly because our structure selection model (4) is able to adaptively preserve more informative structures according to the image characteristics. In addition, the kernel estimates by [1, 3] contain some obvious noise, and the continuity of some kernel estimates also has been destroyed. From these results we can see that our kernel estimation model (11) is able to preserve the continuity of blur kernels, and remove noise in the blur kernels effectively.

In Fig. 7, Sum of Squared Differences Error (SSDE) is employed to compare the estimation accuracy for the blur kernels in Fig. 6. We can see that the accuracy of kernel estimation by proposed method has been greatly

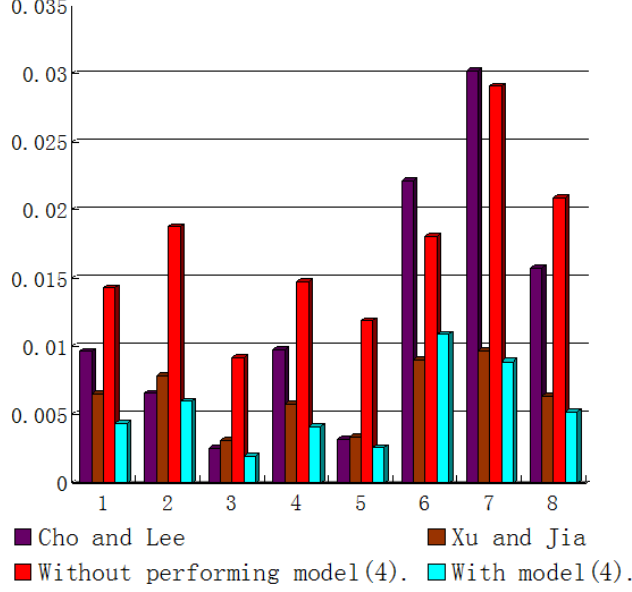


Figure 7: Kernel estimation results comparison in terms of SSDE.

improved.

To furthermore address importance of salient edges ∇S and the effectiveness of our whole kernel estimation algorithm, we conduct another experiment shown in Fig. 8. As can be seen from Fig. 8, the SSDE values of kernel estimates, without adopting salient edges ∇S (i.e., the red curve in Fig. 8), are increasing with the iterations. On the contrary, the results with structure selection methods (i.e., cyan curve and green curve in Fig. 8), performs better. This furthermore demonstrates the importance of salient edges. Compared the cyan curve with the green curve, the quality of kernel estimates, by adopting the structure selection model (4), has been greatly improved, and the accuracy and convergency are better than the methods without adopting model (4). This is also in line with our understanding (Il-

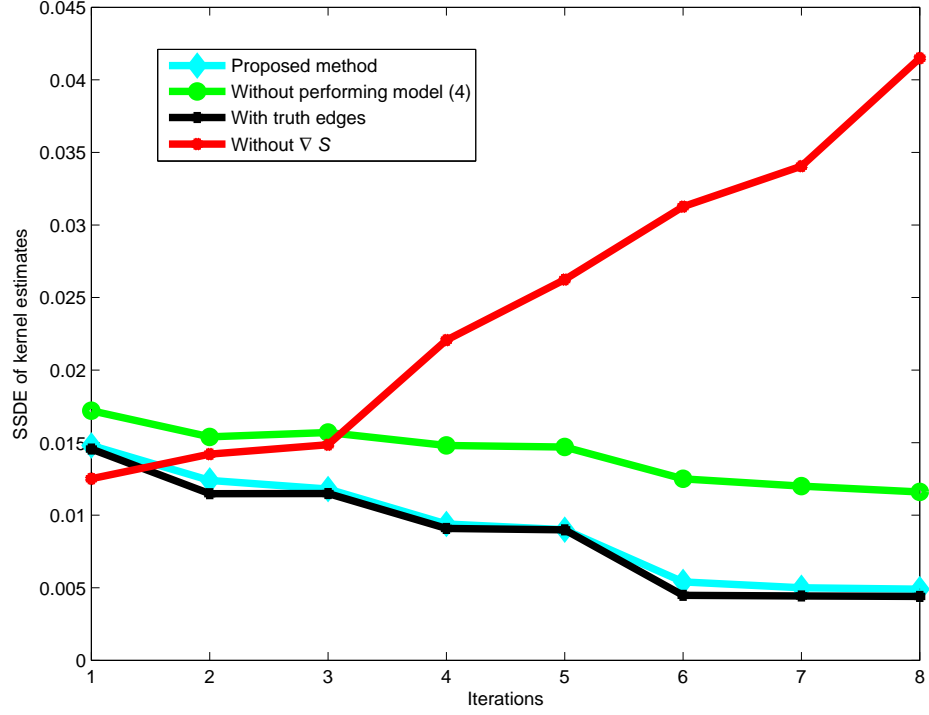


Figure 8: Importance of salient edges ∇S and the effectiveness of our whole kernel estimation algorithm. The red curve shows the kernel estimation errors without adopting any structure selection strategies. The green curve shows the kernel estimation errors without adopting model (4) in the proposed structure selection strategy. The cyan curve shows the kernel estimation errors with the proposed structure selection strategy. The black curve shows the kernel estimation errors with the proposed structure selection strategy, while the salient edges are extracted from truth image.

lustrated in Introduction and Section 3.1). From the cyan curve and black curve, we can see that our salient edges extracted from interim latent images performs comparably to the salient edges extracted from truth images. This verifies the validity of our structure selection method.

In addition, an effective constraint Eq. (10) is introduced to remove noise when reliability of some structures does not be guaranteed. Results shown in Fig. 5 demonstrate such a possibility. More illustrative examples are included in supplemental material.

3.4. Final Latent Image Estimation

Model (14) may lead to the stair-casing effect and destroy textures. To preserve more sharp edges and textures, we make use of our predicted structure to guide the recovery of the latent image. The predicted structure ∇S is utilized as the weight of spatial prior. Thus, our final model for latent image restoration is defined as follows,

$$\min_I \|B - k * I\|_2^2 + \lambda(\exp(-\|\partial_x S\|^{0.8})\|\partial_x I\|_1 + \exp(-\|\partial_y S\|^{0.8})\|\partial_y I\|_1). \quad (15)$$

Both model (14) and (15) can be solved by using IRLS method efficiently.

Based on above analysis, our deblurring algorithm is summarized in Alg. 2.

4. Experimental Results and Evaluation

We compared our method with other state-of-the-art approaches on several challenging examples. In the kernel estimation, all color images are converted to gray ones, the initialized value of θ is set to 1, and t is initialized according to [1]. λ_c in model (14) is set to 0.005, λ in model (15) is set

Algorithm 2 The Completed Image Deblurring Algorithm

Input: Blur image B and the size of blur kernel;

Determine the number of image pyramid n according to the size of kernel;

for $i = 1 \rightarrow n$ **do**

Downsample B according to the current image pyramid, and get B_i ;

for $innerItr = 1 \rightarrow m$ (m iterations) **do**

Select salient edges ∇S according to Eq. (7);

Estimate kernel k according to Alg. 1;

Estimate latent image I_i according to model (14);

$t \leftarrow t/1.1, \theta \leftarrow \theta/1.1$;

end for

Upscale image I_i , and set $I_{i+1} \leftarrow I_i$;

end for

Estimate the final latent image I according to model (15);

Output: Blur kernel k and latent image I .

to 0.003, and γ in model (11) is set to 0.01. In Alg. 1, solving model (13) will produce negative values. We adopt Yuan et al’s method [20] to remove negative values of blur kernels. In the final deconvolution process, each color channel is separately processed.

We first use a synthetic example shown in Fig. 9 to prove the effectiveness of our method. The blurred image contains rich textures and many small details, such as flowers, leaves and grass which increase the difficulty for kernel estimation. We compare our method with state-of-the-art motion deblurring methods [4, 2, 1, 3, 6]. Methods of Fergus *et al.* [4] and Shan *et al.* [2] fail to provide correct kernel estimation results, and their deblurred results still contain some blur and ringing artifacts. Other methods [3, 1, 6] provide deblurred results with some ringing artifacts due to imperfect kernel estimation results. Our results shown in Fig. 9(g) perform well both in the kernel estimation and the final latent image restoration.

In Table 1, we employ SSDE and PSNR (Peak Signal to Noise Ratio) to compare the estimation accuracy for the blur kernels and the restored images in Fig. 9, respectively.

Our method provides higher PSNR value for the restored image. For kernel estimates, our method has lower SSDE value.

Table 1: Comparison of estimated results in Fig. 9.

Methods	[4]	[2]	[1]	[3]	[6]	Ours
PSNR of images	15.45	14.78	14.44	13.47	15.33	19.92
SSDE of kernels	0.2654	0.0329	0.0298	0.0301	0.0292	0.0021

We then test the effectiveness of our structure selection model (4). Fig. 10(a)

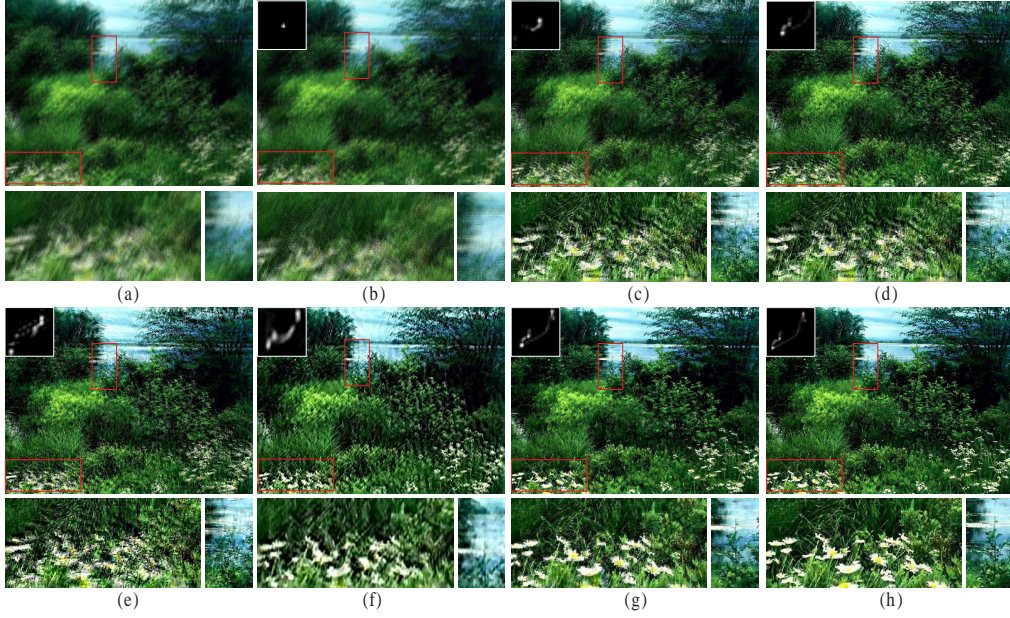


Figure 9: Small tiny details such as the grass and leaves are contained in the image. (a) Blurred image. (b) Result of Fergus *et al.* [4]. (c) Result of Shan *et al.* [2]. (d) Result of Cho and Lee [1]. (e) Result of Xu and Jia [3]. (f) Result of Krishnan *et al.* [6]. (g) Our result. (h) The ground truth result. The size of motion blur kernel is 27×27 .

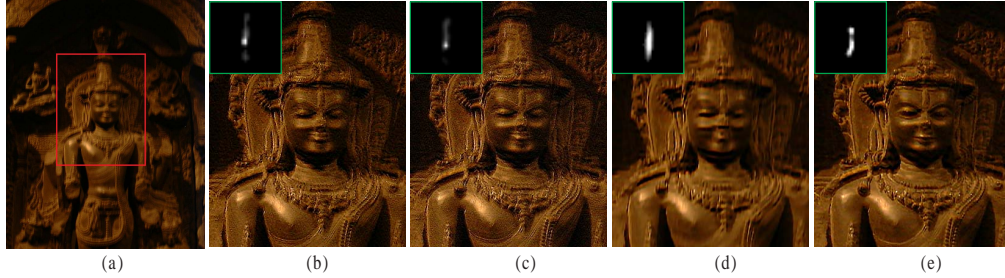


Figure 10: Deconvolution results comparison with and without using image structures. (a) Blurred image. (b-e) are deblurred results cropped from the red box in (a). (b) Result of Shan *et al.* [2]. (c) Result of Cho and Lee [1]. (d) Result without performing model (4). (e) Result with model (4).

is a real captured image presented in [4]. The deblurred results of [2, 1] contain some noises. Fig. 10(d) shows our result without performing model (4), compared with the result shown in Fig. 10(e), its quality is lower, indicating the importance of structures in estimating kernel.

For real images with rich textures and small details, our method can still achieve good results. Fig. 11(a) shows a challenging example with tiny structures in the blurred image (published in [3]). The methods of Fergus *et al.* [4], Shan *et al.* [2], Cho and Lee [1] and Krishnan *et al.* [6] can not obtain accurate deblurred results, and the kernel estimation results. The method of Xu and Jia [3] performs better, but the final deblurred result contains visual artifacts (shown in the red box in Fig. 11(e)), and the kernel estimation result contains some obvious noises. Our method outperforms these methods both in the kernel estimation and the latent image restoration. Comparing the Fig. 11(g) and Fig. 11(h), our simple adaptive weighted spatial prior can preserve more sharp edges and finer textures in the latent image.

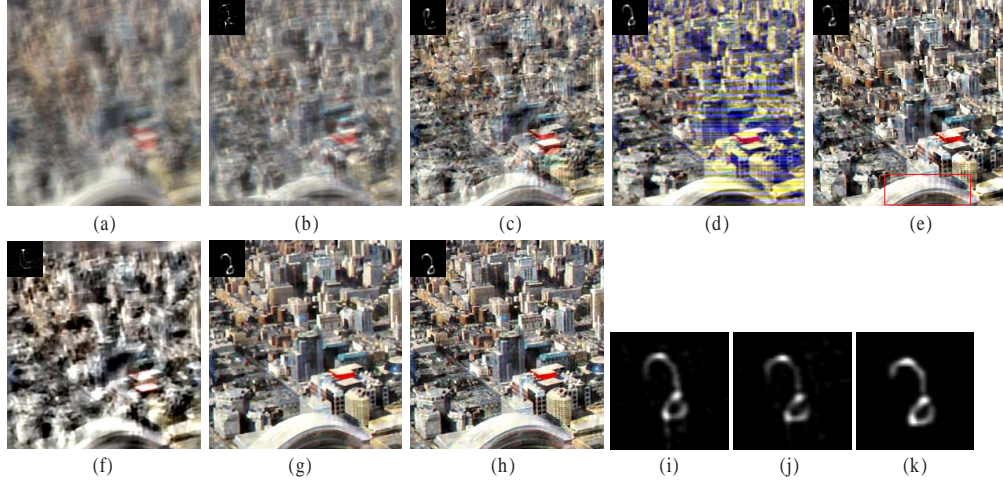


Figure 11: A challenging example with much tiny structures contained in the image. They greatly increase the difficulty of kernel estimation. (a) Blurred image. (b) Result of Fergus *et al.* [4]. (c) Result of Shan *et al.* [2]. (d) Result of Cho and Lee [1]. (e) Result of Xu and Jia [3]. (f) Result of Krishnan *et al.* [6]. (g-h) Our results. Deblurred results in (g) and (h) are generated by model (14) and (15), respectively. (i) Kernel estimate in [1]. (j) Kernel estimate in [3]. (k) Our kernel estimation result. The size of blur kernel is 45×45 .

Another important advantage of our method is that it can deal with large blur kernels. The photo in Fig. 12(a) is captured by ourselves, whose motion blur is quite large. The method of [1] performs better than that of [3], but the kernel estimation result still contains some noises, and the deblurred result is inaccurate in the red box. Due to large blur, methods of [2, 6] cannot also produce correct kernel estimation results and their deblurred results still contain some obvious blur and ringing artifacts (e.g., the part in the red boxes). Our approach, however, generates results that are visually comparable.

Fig. 13 shows another example with large motion blur, and the blurred

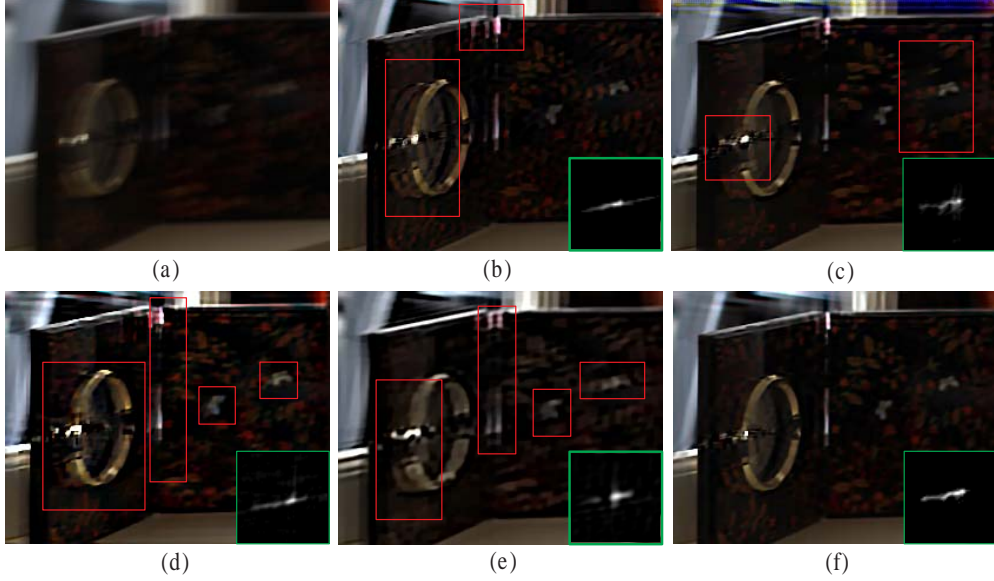


Figure 12: Large blur kernel estimation. (a) Blurred image. (b) Result of Shan *et al.* [2]. (c) Result of Cho and Lee [1]. (d) Result of Xu and Jia [3]. (e) Result of Krishnan *et al.* [6]. (f) Our result. The red boxes shown in (b-e) contain some ringing artifacts. Our estimated blur kernel size is 53×53 .

image also contains small details. Our method provides clearer image with finer textures. Results of [1, 3] still contain some blur.

Evaluation on the Synthetic Dataset [10]: We perform quantitative evaluation of our kernel estimation method by using the dataset from Levin *et al.* [10], and compare our kernel estimation results with the current state-of-the-art blind deconvolution algorithms of Cho and Lee [1], Xu and Jia [3] and Levin *et al.*’s latest method [7]. For evaluation with each test case, we followed the method used in [10]. The kernel estimation results of [1, 3, 10] are all generated by using the authors’ binary codes downloaded online. Then, the deblurred results are obtained by using Levin *et al.*’s matlab function

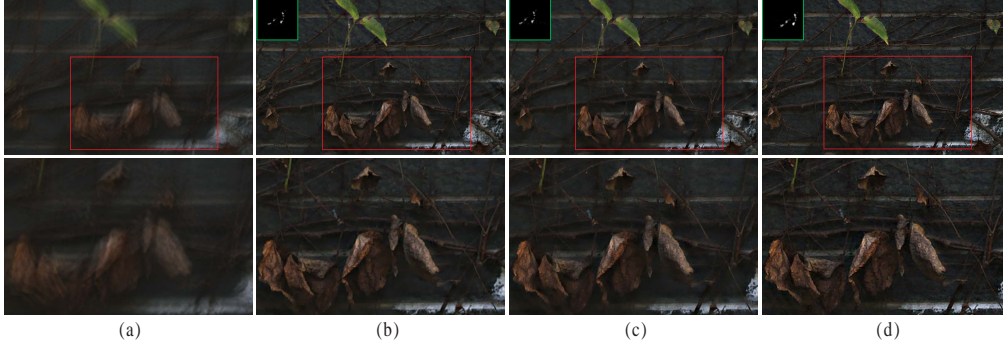


Figure 13: Another large blur kernel estimation example. (a) Blurred image. (b) Result of Cho and Lee [1]. (c) Result of Xu and Jia [3]. (d) Our result. Our estimated blur kernel size is 99×99 .

`deconvSps.m` with the same parameter settings. The error metric is also the same as [10].

In Fig. 14, we plot the cumulative histograms of deconvolution error ratios in the same way as [7]. In the x-axis, a number of n shows the percentage of test cases whose deconvolution error ratios are below n . Our method provides more reliable results than others.

Fig. 15 shows the corresponding kernel estimation results. One can see that our method generates clear and noiseless kernel estimation results. More comparison results can be found in our supplementary materials.

5. Conclusions

In this work, we developed a novel kernel estimation algorithm based on image salient edges. We discovered that image details could undermine the kernel estimation, especially for large blur kernels. Therefore, we propose a self-adaptive algorithm for image structure-texture decomposition, which is

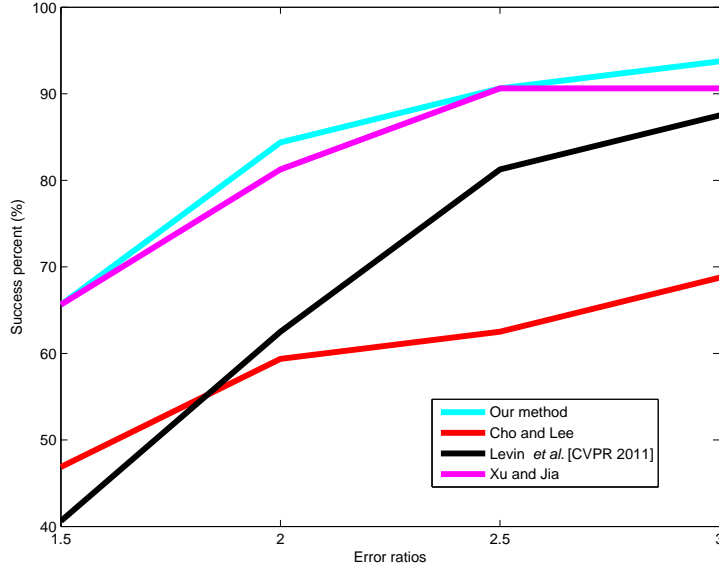


Figure 14: Cumulative histogram of the deconvolution error ratio across test examples.

able to remove structures with potential aversive effects to the estimation. Our kernel estimation model preserves the characteristics of the kernel, such as continuity and sparsity, removes noises, further reduces the aversive effects caused by the wrong chosen structures. In the final deconvolution step, we utilized the structural information for an adaptive weighted regularization term to guide the latent image restoration, which preserves the image details well.

We have extensively tested our algorithm, and found that it is able to deblur images with both small and large blur kernels especially when the blurred images contain rich details.

Although our method achieves excellent results, it has some limitations. One is that the blurred images are textureless, The other is that blurred

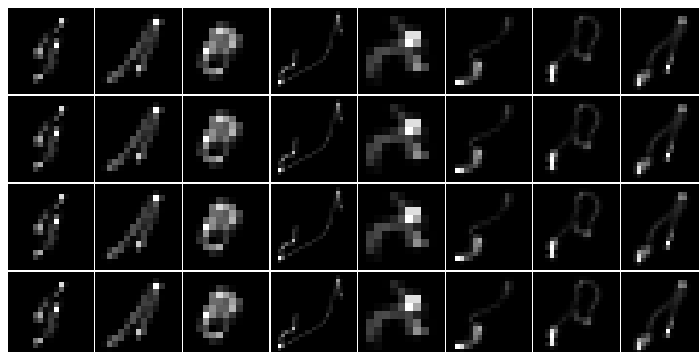
images contains severe noise and many saturated pixels. Dealing with these problems will be our future work.

References

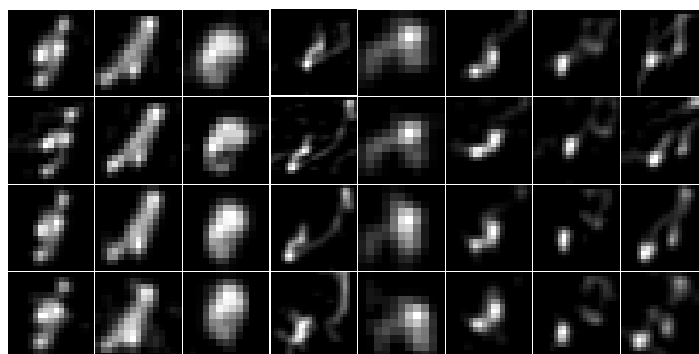
- [1] S. Cho, S. Lee, Fast motion deblurring, *ACM Transactions on Graphics (SIGGRAPH Asia)* 28 (5) (2009) 1–8.
- [2] Q. Shan, J. Jia, A. Agarwala, High-quality motion deblurring from a single image, *ACM Transactions on Graphics* 27 (3) (2008) 1–10.
- [3] L. Xu, J. Jia, Two-phase kernel estimation for robust motion deblurring, in: *ECCV*, 2010, pp. 157–170.
- [4] R. Fergus, B. Singh, A. Hertzmann, S. T. Roweis, W. T. Freeman, Removing camera shake from a single photograph, *ACM Transactions on Graphics* 25 (3) (2006) 787–794.
- [5] N. Joshi, R. Szeliski, D. J. Kriegman, Psf estimation using sharp edge prediction, in: *CVPR*, 2008, pp. 1–8.
- [6] D. Krishnan, T. Tay, R. Fergus, Blind deconvolution using a normalized sparsity measure, in: *CVPR*, 2011, pp. 2657–2664.
- [7] A. Levin, Y. Weiss, F. Durand, W. T. Freeman, Efficient marginal likelihood optimization in blind deconvolution, in: *CVPR*, 2011, pp. 2657–2664.
- [8] W. G. Chen, N. Nandhakumar, W. N. Martin, Image motion estimation from motion smear-a new computational model, *IEEE Transactions on Pattern Analysis Machine Intelligence* 18 (1) (1996) 234–778.

- [9] T. Chan, C. Wong, Total variation blind deconvolution, *IEEE Transactions on Image Processing* 7 (3) (1998) 370–375.
- [10] A. Levin, Y. Weiss, F. Durand, W. T. Freeman, Understanding and evaluating blind deconvolution algorithms, in: *CVPR*, 2009, pp. 1964–1971.
- [11] Y. Wang, W. Yin, Compressed sensing via iterative support detection, Tech. rep., Rice CAAM Technical Report TR09-30 (2009).
- [12] L. B. Lucy, An iterative technique for the rectification of observed distributions, *Astronomy Journal* 79 (6) (1974) 745–754.
- [13] A. Levin, R. Fergus, F. Durand, W. T. Freeman, Image and depth from a conventional camera with a coded aperture, *ACM Transactions on Graphics* 26 (3) (2007) 70–78.
- [14] Y. Wang, J. Yang, W. Yin, Y. Zhang, A new alternating minimization algorithm for total variation image reconstruction, *SIAM Journal on Imaging Sciences* 1 (3) (2008) 248–272.
- [15] L. I. Rudin, S. Osher, E. Fatemi, Nonlinear total variation based noise removal algorithms, *Physica D* 60 (1992) 259–268.
- [16] S. Osher, L. I. Rudin, Feature-oriented image enhancement using shock filters, *SIAM Journal on Numerical Analysis* 27 (4) (1990) 919–940.
- [17] T. S. Cho, S. Paris, B. K. P. Horn, W. T. Freeman, Blur kernel estimation using the radon transform, in: *CVPR*, 2011, pp. 241–248.

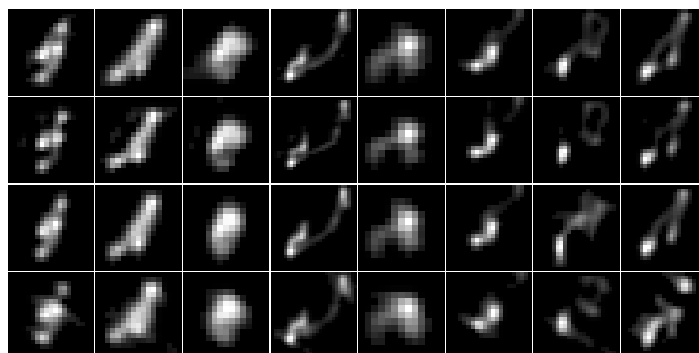
- [18] J. Chen, L. Yuan, C. K. Tang, L. Quan, Robust dual motion deblurring, in: CVPR, 2008, pp. 1–8.
- [19] L. Xu, C. Lu, Y. Xu, J. Jia, Image smoothing via l_0 gradient minimization, ACM Transactions on Graphics (SIGGRAPH Asia) 30 (6) (2011) 1–11.
- [20] L. Yuan, J. Sun, L. Quan, H.-Y. Shum, Image deblurring with blurred/noisy image pairs, ACM Transactions on Graphics 26 (3) (2007) 1–10.



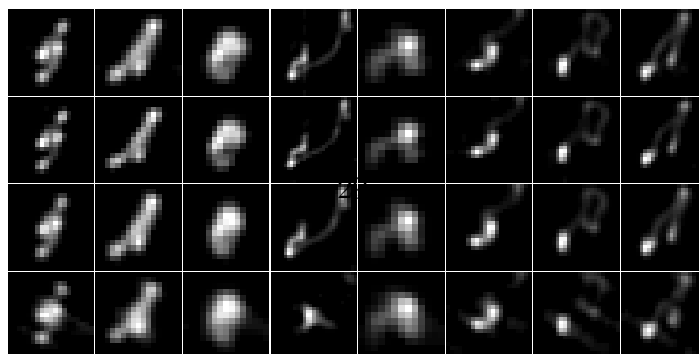
(a) Truth kernels



(b) Cho and Lee [1]



(c) Xu and Jia [3]



(d) Our result